Available online at www.sciencedirect.com
SCIENCE DIRECT®
Journal of Nuclear Materials 352 (2006) 190–195
journal of nuclear materials
www.elsevier.com/locate/jnucmat

Kinetics of iron redox reactions in silicate liquids: A high-temperature X-ray absorption and Raman spectroscopy study

V. Magnien [a,b], D.R. Neuville [a,*], L. Cormier [c], J. Roux [a], J.-L. Hazemann [d], O. Pinet [b], P. Richet [a]

[a] *Physique des Minéraux et Magmas, CNRS-IPGP, 4 place Jussieu, 75252 Paris cedex 05, France*
[b] *CEA VALRHO Marcoule, SCDV, LEBV, BP 17171, 30207 Bagnols/Cèze, France*
[c] *IMPMC, CNRS UMR 7590, Universités Paris 6 and 7 and IPGP, 4 place Jussieu, 75252 Paris cedex 05, France*
[d] *Laboratoire de cristallographie, UPR 5031, CNRS, 38043 Grenoble, France*

Abstract

The oxidation kinetics of a Fe-bearing supercooled liquid of the system SiO_2–CaO–MgO–Na_2O–FeO has been determined near the glass transition range by X-ray absorption near edge structure (XANES) and Raman spectroscopies. Both techniques yield room-temperature iron redox ratios in accord with wet chemical, Mössbauer and electron microprobe analyses. Similar oxidation kinetics have also been observed with both methods. At constant temperature, the kinetics obey an exponential law with a characteristic time that follows an Arrhenian temperature dependence. As redox changes are too fast to be accounted for in terms of diffusion of either ionic or molecular oxygen, these results lend further support to the idea that the rate-limiting factor for oxidation near the glass transition is diffusion of network-modifying cations along with a flux of electron holes.

PACS: 81.65.Mq; 61.43.Fs; 61.10.Ht

1. Introduction

Silicate glasses owe their interest for long-term nuclear waste disposal to their lack of long-range order and the ensuing possibility of incorporating a great many chemical elements. When multivalent elements are present, however, the physical and chemical properties of the glass can depend markedly on redox state. For iron, much work has been devoted to equilibrium redox ratios [1–3] but the kinetics of redox changes remain poorly known in spite of the practical importance of these reactions in glass making. Kinetic studies are in addition of fundamental interest because of the information they yield on redox mechanisms through determination of rate-limiting parameters. Whereas diffusion of oxygen in the form of O_2 or O^{2-} was first considered [4–6], recent studies favor instead diffusion of

* Corresponding author. Tel.: +33 1 44 27 43 47; fax: +33 1 44 27 24 87.
E-mail address: neuville@ipgp.jussieu.fr (D.R. Neuville).

0022-3115/$ - see front matter © 2006 Elsevier B.V. All rights reserved.
doi:10.1016/j.jnucmat.2006.02.053

divalent cations coupled to a flux of electron holes [7–9].

From a practical standpoint, redox studies have hitherto suffered from the paucity of suitable methods to determine in situ either the redox ratio ($r = Fe^{3+}/Fe_{tot}$) or the structural state of iron. In fact, both Fe^{3+}/Fe_{tot} and oxygen coordination around iron ions in silicate minerals and glasses can be determined by X-ray absorption near edge structure (XANES) spectroscopy [10–14]. Recently, we have shown that such measurements lend themselves to kinetic studies since they can be readily performed at high-temperatures [15]. Because the effects of time and temperature on redox kinetics were not distinguished in our preliminary work, here we present new, systematic measurements made as a function of time at constant temperature. These observations were again made near the glass transition where discrimination between possible rate-limiting factors is made easier by the slower kinetics of the redox reaction.

Raman spectroscopy is another technique extensively used to derive structural information on silicate glasses and melts as a function of composition [16–18]. Although bands between 800 and 1200 cm^{-1} are sensitive to the iron redox state [19,20], a detailed study of this effect is lacking. Another goal of this contribution is thus to show that consistent and complementary results concerning iron redox state and mechanisms can be obtained from Raman spectra.

2. Experimental methods

2.1. Samples

The compositions and names of the glasses investigated are listed in Table 1. These glasses are the same as in our preliminary study [15] to which we refer for more details on sample preparation. The PyrNa starting glass was synthesized from an oxide and carbonate mix heated in air at 1873 K in a platinum crucible. We obtained the more oxidized samples PyrNa750 and PyrNa1200 by annealing for three weeks in air mm-size chunks of PyrNa, kept in platinum crucibles at 1023 and 1473 K, respectively. The strongly reduced PyrNa5R and PyrNa17R samples were prepared through remelting of PyrNa in a graphite crucible during 5 and 17 min, respectively. No evidence for partial crystallization of the samples, either before or after the experiment, was found in the Mössbauer and Raman spectra or in XANES pre-edges features [13].

Glass transition temperatures (T_g) were first measured for two samples to determine the temperature range at which the kinetic measurements were to be made. We determined temperatures of 889 K for PyrNa from viscosity experiments [21] and of 883 K for PyrNa17R from heat capacities measured with a Sétaram-121 differential scanning calorimeter. The value of T_g is marginally lower for the most reduced sample, but is coherent with the fact that

Table 1
Chemical composition, density and room-temperature redox ratio of the starting materials

	PyrNa	PyrNa17R	PyrNa5R	PyrNa750	PyrNa1200
Chemical composition (wt %)[a]					
SiO_2	52.60 (±0.05)	52.78 (±0.1)	52.58 (±0.1)	52.69 (±0.1)	52.47 (±0.2)
MgO	11.98 (±0.05)	11.99 (±0.04)	11.91 (±0.03)	11.99 (±0.02)	11.60 (±0.1)
CaO	17.01 (±0.03)	17.00 (±0.03)	16.94 (±0.02)	17.08 (±0.06)	16.48 (±0.1)
Na_2O	5.46 (±0.01)	5.48 (±0.02)	5.53 (±0.02)	5.42 (±0.05)	5.93 (±0.2)
FeO[b]	12.83 (±0.03)	12.75 (±0.1)	12.92 (±0.1)	12.68 (±0.05)	13.52 (±0.1)
Density (g cm^{-3})[c]	2.912	2.828	2.907	2.914	2.915
Redox ratio (wt %) Fe^{3+}/Fe_{tot}					
Wet chemistry (±0.02)	0.75	0.09	0.62	0.98	0.90
Mössbauer (±0.02)	0.75	0.09	0.60	0.93	0.95
Microprobe (±0.07)	0.69	0.10	0.60	0.91	0.82
XANES (±0.05)	0.78	0.05		0.99	0.90
Raman (±0.05)	0.75	0.09[d]	0.63	0.99[d]	0.94

[a] Average of 15–20 analyses made on different glass fragments with a Cameca SX100 microprobe.
[b] All iron reported as FeO.
[c] Densities measured with an Archimedean method and toluene as the immersion liquid.
[d] Assumed value for the endmember when calculating the redox state of intermediate compositions.

ferrous iron usually acts as a network modifier [18] and depolymerizes the silicate network.

As a check of our procedures, we compare in Table 1 the iron redox ratios derived at room temperature from our XANES and Raman observations with the values determined from three other techniques [14]. These include wet chemical analyses [22], Mössbauer spectroscopy observations (made by B.O. Mysen at 90 K on 0.2 g powdered samples with a ^{57}Co source and a standard α-Fe foil for calibration according to Virgo and Mysen [23]), and electron microprobe analyses (performed with a Cameca SX100 probe from the shift of the LIII peak position of iron [24] which was measured eight times at the same point and then extrapolated to zero time [15]). To within their experimental errors, these results are mutually consistent with the exception of a few electron microprobe measurements, which were beset by iron reduction under the electron beam.

2.2. Spectroscopy measurements

For high-temperature XANES and Raman observations, samples were ground under alcohol as a 0.5–1 μm powder before being gently compacted to a 400 μm thickness in the 1-mm hole of the Pt heating wire of a microfurnace [27]. The XANES spectra at the Fe K-edge were recorded in transmission mode at the BM30B FAME beamline of ESRF (Grenoble, France). The ring conditions were 6.0 GeV with injection currents of 200 mA in a uniform filling mode. The X-ray energy was monochromatized with a double sagitally focusing Si(220) crystal. We scanned stepwise in 90 s the photon energy between 7100 and 7300 eV by changing the Bragg angle of the monochromator. After normalization with the Xafs@ software [25], we analyzed the XANES spectra with standard procedures [11,13]. A spline function was used to interpolate the background over several eV intervals below and above the pre-edge [13,14]. The intensity and centroid position of the pre-edge was calculated from a fit to the data made with 2 or 3 pseudo-Voigt functions, see Fig. 1 of [15]. The Fe^{3+}/Fe_{tot} ratio was finally determined from the calibration of these parameters established for a variety of minerals [13].

Unpolarized Raman spectra were recorded with a T64000 Jobin–Yvon confocal microRaman spectrometer equipped with a CCD detector. The 514.532 nm line of a Coherent 70 Ar^+ laser operating at 2 W was the excitation source. For reference glasses and kinetic experiments, we recorded the spectra between 20 and 1500 cm^{-1} or 200 and 1500 cm^{-1}, respectively, in 240 or 600 s for each range. The spectra were corrected for temperature- and frequency-dependent scattering intensity as described by Long [26] and then normalized to the data point of highest intensity. To prevent high-temperature crystallization under the laser beam, all spectra were recorded on samples quenched in a few seconds to room temperature after annealing.

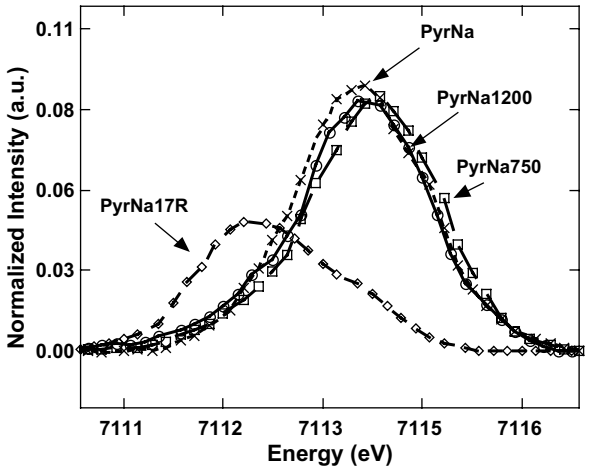

Fig. 1. Differences in iron pre-edges in XANES spectra between oxidized and reduced PyrNa glasses at room temperature.

3. Results and discussion

3.1. Room-temperature redox analyses

In XANES experiments, we focused our attention to the pre-edge region which is most sensitive to the iron redox state and oxygen coordination through the state of the 3d orbital [13]. For PyrNa glasses with differing redox ratios (Fig. 1), this feature does show important differences under ambient conditions. The pre-edge of PyrNa17R is made up of a strong contribution near 7112 eV along with a weak shoulder at higher energy, whereas that of PyrNa750 shows an intense contribution near 7114 eV. These observations indicate that the PyrNa17R and PyrNa750 samples are mostly reduced and totally oxidized, respectively. The pre-edge of PyrNa1200 is similar to that of PyrNa750, implying that the redox state of both samples are comparable. Finally, the pre-edge of PyrNa is intermediate between the extreme features of PyrNa17R and PyrNa750. The redox ratios determined from these

observations agree with the data determined by other methods (Table 1), confirming that XANES spectroscopy is a reliable probe of iron redox state in glasses [11,13].

The coordination number of iron in PyrNa17R and PyrNa750 was also estimated with the model of Wilke et al. [13] from the pre-edge intensity and centroid position. A noncentrosymetric site such as tetrahedral is usually characterized by more intense pre-edges [10–13]. In agreement with Mössbauer data, we found in both instances Fe^{2+} in octahedral and Fe^{3+} in tetrahedral coordination. The latter is consistent with stabilization of Fe^{3+} in this structural position by a charge-compensating alkali element (see [19]).

The Raman spectra of quenched PyrNa glasses present two characteristic regions (Fig. 2). Between 400 and 800 cm^{-1}, the bands are usually assigned to vibrations involving bridging oxygens (i.e., ^0O–Si–O^0 linkages) [17,19,28] or to the motions of Si against its tetrahedral cage with a slight displacement of oxygens [17]. Between 800 and 1200 cm^{-1}, the high-frequency envelope is associated with symmetric T–O stretching ($T = Si^{4+}$, Al^{3+}, Fe^{3+}) and, consequently, with the various tetrahedral Q^n-species where n is the number of bridging oxygen per tetrahedrally coordinated cation T. Because charge compensation by an alkali cation allows Fe^{3+} to substitute for Si^{4+} as a network former, the sensivity of Raman bands to the polymerization of the silicate network can represent a probe of the iron redox state.

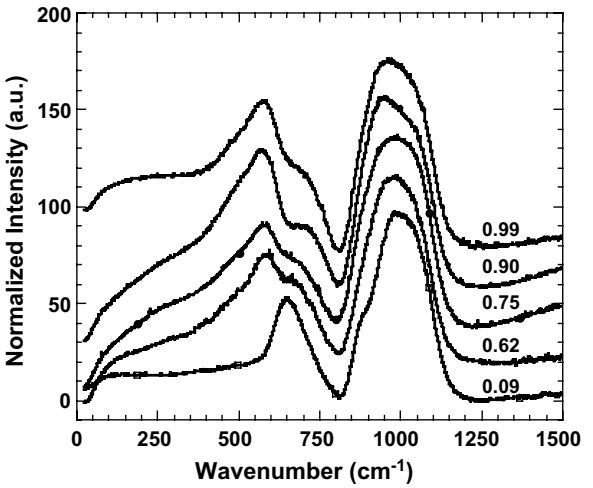

Fig. 2. Room-temperature Raman spectra of PyrNa glasses with the indicated redox ratios as determined from wet chemical analyses.

With increasing iron oxidation, we did observe relative increases of the bands of PyrNa glasses whose maxima lie near 570–590 cm^{-1} and 910 cm^{-1} (Fig. 2). Interestingly, these variations are large enough to allow the redox state of the intermediate compositions to be derived from those of the most oxidized and reduced samples. As a starting point, we have simply determined which linear combination of the broad 800–1200 cm^{-1} band recorded for PyrNa17R and PyrNa750 reproduces best the intensities observed for the intermediate glasses. Agreement with the results derived from other methods is surprisingly good (Table 1), suggesting errors of less than 0.05 for the derived redox ratios. Whenever oxidation is accompanied with a change from 6-fold oxygen coordination for Fe^{2+} to 4-fold for Fe^{3+}, Raman spectroscopy can thus be used to determine changes in redox ratio. Without such a coordination change, however, the validity of this procedure is not warranted. In addition, further work remains to be done to use Raman spectroscopy as a direct means for determining redox ratios since the simple approach followed here requires knowing the redox state of endmembers.

3.2. Kinetics of iron redox changes

To determine the kinetics of the oxidation reaction, we studied the most reduced sample, namely, PyrNa17R, since the Fe^{3+} valence is favored near the glass transition range. Starting from the same redox ratio ($r = 0.09$), we recorded spectra as a function of time between 685 and 983 K and from 873 to 973 K in XANES and Raman experiments, respectively. Even below T_g, the time-dependence of both kinds of spectra caused by changes in the iron redox state is significant at each temperature investigated. Owing to time limitations, however, redox equilibrium was reached only above about 873 K as indicated by the approach to a time-independent value.

The changes of XANES pre-edge features at 938 K with time and the resulting evolution of the redox ratio derived thereof are shown in Fig. 3. At 938 K, time-dependent oxidation is for example discernible through a decrease of the low-energy contribution (Fe^{2+}) and an increase of the high-energy contribution (Fe^{3+}) to the pre-edge (Fig. 3(a)). These changes translate to a progressive increase of Fe^{3+}/Fe_{tot} from 0.09 to the equilibrium value of 0.99 (Fig. 3(b)).

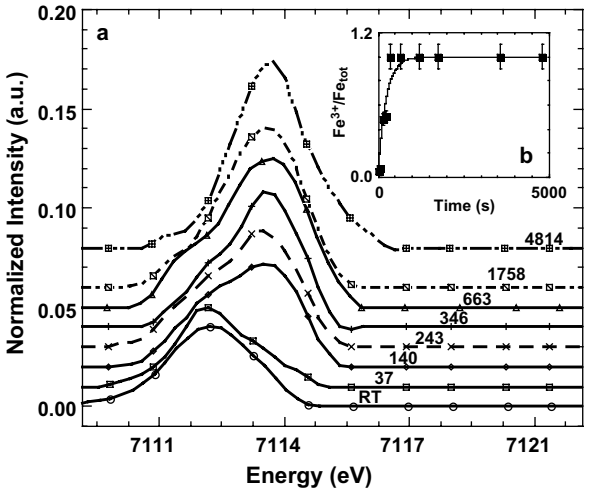

Fig. 3. (a) Evolution of the XANES pre-edges of PyrNa17R heated at 938 K in air; the annealing times are indicated in seconds. (b) Redox ratio against time in this series of measurements.

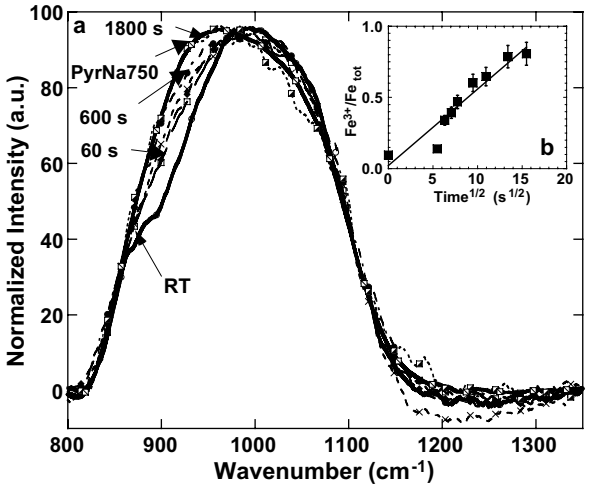

Fig. 4. (a) Evolution of the Raman spectra of PyrNa17R heated in air at 923 K in air during several times. (b) Redox ratio against the square root of time in this series of measurements.

As expected, the kinetics of the redox reaction under isothermal conditions are faster at higher temperatures. The rate of these reactions can be described by expressions of the form used to derive relaxation times, viz.

$$(r_t - r_e) = (r_0 - r_e)\exp(-t/\tau), \quad (1)$$

where r_0 and r_e are the initial and equilibrium redox ratios, r_t the ratio at time t, and τ a characteristic time. In all cases, the redox observations can be accounted for with a constant τ value (see Fig. 3(b)). The values obtained in this way for τ are plotted in an Arrhenian diagram (Fig. 5).

A similar procedure has been followed in Raman spectroscopy. Significant modifications of the spectra were observed with time as illustrated for a temperature of 923 K in Fig. 4. The intensity of the 910 cm^{-1} band clearly increases to reach that found in the spectrum of the reference PyrNa750 glass. In other words, the Fe^{3+}/Fe_{tot} ratio varies with time from 0.09 to reach the equilibrium 0.99 value. As made for the XANES results, expressions of the form (1) have been fitted to the results to determine the characteristic time of the reaction. Again, good agreement is found in Fig. 5 with the analogous XANES results. The Arrhenian nature of the temperature dependence of these characteristic times is also apparent in this figure. The redox kinetics observed with both techniques are the same even though XANES and Raman experiments were made in transmission and reflexion, respectively.

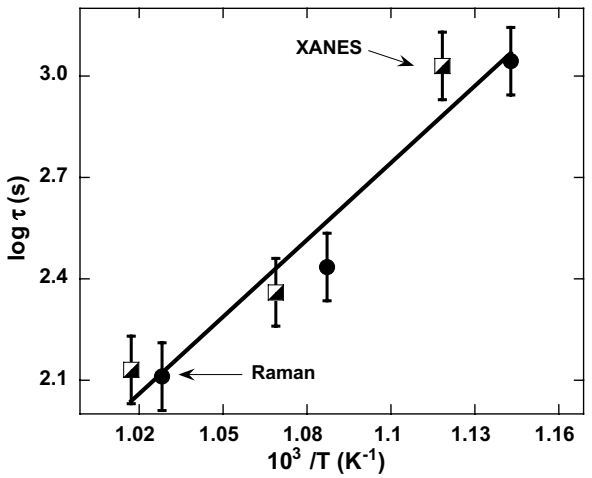

Fig. 5. Temperature dependence of the characteristic time of Eq. (1) as determined from Raman and XANES measurements.

The reason is that, in both cases, the sample was actually probed at the scale of the grain size of less than 1 μm. It thus follows that XANES and Raman spectroscopy can be coupled to provide information on redox reactions and especially on their mechanisms.

Alternatively, redox ratios can be considered to be linear functions of the square root of time (see Fig. 4(b)). Such a relationship indicates that redox reactions are limited by diffusional mechanisms [6,9], and that the time needed to achieve redox equilibrium can be estimated from available diffusion coefficients. By extrapolating available data

down to 923 K for chemical diffusion of oxygen [29] and for diffusion of divalent cations [9], we estimate that D_{O_2} and D_{cat} are 5.5×10^{-15} and 1.3×10^{-13} cm^2 s^{-1}, respectively. From our viscosity data and Eyring's relationship, we find a diffusivity of ionic oxygen of about 2.6×10^{-17} cm^2 s^{-1}. With the relation $t = R^2/4D$, where t is the time needed to achieve equilibrium through diffusion and R is the radius of spherical grains (i.e., 0.25 μm), these diffusivities in turn yield values for t of 3×10^4, 10^3 and 6×10^6 s from D_{O_2}, D_{cat} and D_{O_2-}, respectively.

On the other hand, our experiments yield a value of t of 10^3 s to achieve equilibrium at 923 K. Hence, diffusion of molecular and ionic oxygen seems too low to control redox reactions near the glass transition. In contrast, diffusion of divalent cations is consistent with the timescale of our kinetic experiments. We thus conclude that diffusion of network modifying cations controls the iron redox mechanism. This conclusion agrees with those of previous 'static' studies [8–10], and also with the inferences drawn in our previous work where the effects of time and temperature on the redox kinetics were not clearly separated [15]. They are also consistent with the decoupling observed near the glass transition between the relaxation of silicate network and the mobility of divalent cations [30].

Acknowledgements

We thank O. Proux (ESRF) for help with the XANES experiments, B.O. Mysen from Geophysical laboratory (Carnegie Institution of Washington) for the Mössbauer analyses and fruitful discussions, and M. Fialin from Camparis (Université Paris VI) for the electron microprobes analyses. IPGP contribution no. 2127.

References

[1] V.C. Kress, I.S.E. Carmichael, Am. Min. 73 (1988) 1267.
[2] V.C. Kress, I.S.E. Carmichael, Contrib. Mineral. Petrol. 108 (1991) 82.
[3] O. Pinet, C. DiNardo, in: Proc. 101th Meet. Am. Ceram. Soc., Electrochem. Mat. Dev. Ceram. Trans., vol. 109, 1999, p. 367.
[4] D.S. Goldman, P.K. Gupta, J. Am. Ceram. Soc. 66 (1983) 188.
[5] H.D. Schreiber, S.J. Kozak, A.L. Fritchman, D.S. Goldman, H.A. Schaeffer, Phys. Chem. Glasses 27 (1986) 152.
[6] R.F. Wendlandt, Contrib. Mineral. Petrol. 108 (1991) 463.
[7] G.B. Cook, R.F. Cooper, J. Non-Cryst. Solids 120 (1990) 207.
[8] R.F. Cooper, J.B. Fanselow, D.B. Poker, Geochim. Cosmochim. Acta 60 (1996) 3253.
[9] G.B. Cook, R.F. Cooper, Am. Min. 85 (2000) 397.
[10] S. Bajt, S.R. Sutton, J.S. Delaney, Geochim. Cosmochim. Acta 58 (1994) 5209.
[11] L. Galoisy, G. Calas, M.A. Arrio, Chem. Geol. 174 (2001) 307.
[12] M. Bonnin-Mosbah, A.S. Simionovici, N. Métrich, J.P. Duraud, D. Massare, P. Dillmann, J. Non-Cryst. Solids 288 (2001) 103.
[13] M. Wilke, F. Farges, P.E. Petit, G.E. Brown Jr., F. Martin, Am. Min. 86 (2001) 714.
[14] A.J. Berry, H.St.C. O'Neill, K.D. Jayasuriya, S.J. Campbell, G.J. Foran, Am. Min. 88 (2003) 967.
[15] V. Magnien, D.R. Neuville, L. Cormier, B.O. Mysen, V. Briois, S. Belin, O. Pinet, P. Richet, Chem. Geol. 213 (2004) 253.
[16] B.O. Mysen, D. Virgo, F.A. Seifert, Rev. Geophys. 20 (1982) 353.
[17] P. McMillan, Am. Min. 69 (1984) 622.
[18] B.O. Mysen, P. Richet, Silicate Glasses and Melts: Properties and Structure, Elsevier, Amsterdam, 2005, 544 p.
[19] B.O. Mysen, F.A. Seifert, D. Virgo, Am. Min. 65 (1980) 867.
[20] Z. Wang, T.F. Cooney, S.K. Sharma, Geochim. Cosmochim. Acta 59 (1995) 1571.
[21] D.R. Neuville, P. Richet, Geochim. Cosmochim. Acta 55 (1991) 1011.
[22] A.D. Wilson, Analyst 85 (1960) 823.
[23] D. Virgo, B.O. Mysen, Phys. Chem. Min. 12 (1985) 65.
[24] M. Fialin, C. Wagner, N. Metrich, E. Humler, L. Galoisy, A. Bezos, Am. Min. 86 (2001) 456.
[25] M. Winterer, J. Phys. IV C2 (1997) 243.
[26] D.A. Long, Raman Spectroscopy, McGraw-Hill, New York, 1977, 276 p.
[27] P. Richet, P. Gillet, A. Pierre, M.A. Bouhifd, I. Daniel, G. Fiquet, J. Appl. Phys. 74 (1993) 5451.
[28] B.O. Mysen, D. Virgo, E.R. Neumann, F.A. Seifert, Am. Min. 70 (1985) 317.
[29] K.W. Semkow, L.A. Haskin, Geochim. Cosmochim. Acta 49 (1985) 1897.
[30] G. Gruener, P. Odier, D. De Sousa Meneses, P. Florian, P. Richet, Phys. Rev. B 64 (2001) 024206/1.